Development of a Terahertz Metamaterial Micro-Biosensor for Ultrasensitive Multispectral Detection of Early Stage Cervical Cancer

Musa N. Hamza, Mohammad Tariqul Islam, *Senior Member, IEEE*, Sunil Lavadiya, *Member, IEEE*, Iftikhar ud Din, Bruno Cavalcante de Souza Sanches, *Member, IEEE*, Slawomir Koziel, *Fellow, IEEE*, Syeda Iffat Naqvi, *Senior Member, IEEE*, Ali Farmani, *Member, IEEE*, and Md. Shabiul Islam, *Senior Member, IEEE*

***Abstract*—This research introduces an innovative design for a metamaterial (MTM)-based compact multiband biosensor aimed at early stage cervical cancer detection. The device operates within the terahertz (THz) frequency range, specifically from 0 to 6 THz. The proposed sensor architecture features an MTM layer composed of a patterned aluminum structure deposited on a polyimide substrate. The primary design objective is to optimize the geometry parameters to achieve near-perfect absorption of electromagnetic (EM) waves across the entire operating bandwidth. The design process utilizes full-wave EM simulation tools. This article details all intermediate steps in the sensor's topology development, guided by an investigation of the absorption characteristics of successive architectural variations. It also analyzes the effects of the substrate and resonator material. The suitability of the proposed sensor for early stage cancer diagnosis is demonstrated using a microwave imaging (MWI) system that incorporates the device. Extensive simulation studies confirm the sensor's capability to distinguish between healthy and cancerous cervical tissue. For further validation, comprehensive benchmarking is conducted against numerous state-of-the-art sensor designs reported in recent literature. These comparative studies indicate that the proposed sensor offers superior performance in terms of absorbance levels and the width of the operating bandwidth, both of which enhance the sensitivity of cancer detection.**

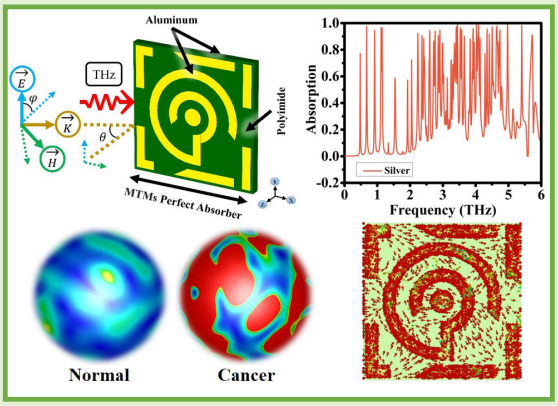

***Index Terms*— Biosensor, cervical cancer, metamaterials (MTMs), microwave imaging (MWI), multiband sensors.**

I. Introduction

TERAHERTZ (THz) waves possess a range of unique advantages that make them highly promising for various applications, particularly in biological detection and pharmaceutical fields. The combination of low photon energy and strong penetration ability akin to X-rays makes THz waves particularly well suited for exploring biological tissues and molecules. One of the key advantages of THz technology lies in its ability to perform label-free, nondestructive, and noncontact detection, thus preserving the integrity of analyte for further analysis [1], [2]. Furthermore, THz sensors offer real-time monitoring capabilities, enabling researchers to observe dynamic biological processes as they unfold [3]. This real-time feedback is invaluable in pharmacological applications, where rapid assessment of drug interactions and effects is critical for developing effective treatments. Moreover, the nontoxic and nondestructive nature of THz waves to human tissue makes them safer for use in medical diagnostics compared to other techniques that may involve ionizing radiation or invasive procedures, thus minimizing potential health risks associated with diagnostic procedures [4]. Overall, the unique properties of THz technology, including its noninvasive

Manuscript received 18 June 2024; revised 8 August 2024; accepted 18 August 2024. Date of publication 11 September 2024; date of current version 16 October 2024. This work was supported in part by the Ministry of Higher Education (MOHE), Malaysia, through the Fundamental Research Grant Schemes (FRGS) under Grant FRGS/1/2021/TK0/UKM/01/6; in part by the Icelandic Research Fund under Grant 239858; and in part by the National Science Centre of Poland under Grant 2020/37/B/ST7/01448. The associate editor coordinating the review of this article and approving it for publication was Dr. Shyqyri Haxha. *(Corresponding authors: Musa N. Hamza; Mohammad Tariqul Islam; Md. Shabiul Islam.)*

Please see the Acknowledgment section of this article for the author affiliations.

Digital Object Identifier 10.1109/JSEN.2024.3447728

nature, real-time monitoring capabilities, and ability to provide detailed information about biological samples, position it as a highly promising tool for a wide range of applications in biomedical research, pharmaceutical development, and clinical diagnostics.

Metamaterials (MTMs) represent a cutting-edge class of artificial electromagnetic (EM) materials constructed from subwavelength units arranged in a periodic array. These materials are engineered to exhibit unique EM properties not found in naturally occurring substances such as negative refractive index and negative permittivity. These properties enable MTMs to manipulate EM waves in unconventional ways, leading to applications such as absorbers [5], active filters [6], and ultrasensitive biosensors [7], [8], [9], [10]. In addition, MTMs can exhibit inverse Doppler effects [11], which opens up new possibilities in signal processing and communication systems. Resonant MTMs, in particular, possess microsized gaps that enable them to concentrate and enhance the intensity of local EM fields. This enhancement is advantageous for applications requiring high sensitivity to changes in dielectric properties, making resonant MTMs particularly well suited for THz sensing. In THz sensing, the ability to detect minute changes in dielectric properties is crucial for identifying and analyzing biomolecules, chemical substances, and other materials [12]. By leveraging the enhanced sensitivity provided by resonant MTMs, THz sensors can achieve higher accuracy and resolution in detecting and characterizing samples [13]. Overall, the unique EM properties of MTMs, particularly resonant MTMs, make them powerful tools for advancing THz sensing technologies and opening up new possibilities in fields such as biomedical diagnostics specifically cancer cell sensing [14], [15] and chemical sensing [16], [17], [18], [19], [20], [21], [22], environmental monitoring, materials science, and communication systems.

With millions of new cases diagnosed each year and a substantial number of deaths attributed to the disease, cancer remains a major public health concern worldwide and also a foremost inhibitor to increasing life expectancy. The World Health Organization (WHO) report for global cancer data released in 2020 indicated an estimated number of 19.29 million new cancer cases worldwide, including 9.96 million deaths. It is expected this number of new cases to increase to 28.4 million in 2040 [23], [24]. Efforts to address cancer incidence and mortality include not only advancements in treatment methods but also initiatives focused on prevention, early detection, and improving access to healthcare services. The existing techniques, such as electrochemical methods, histopathological or immunological methods, fluorescence imaging, and cytometry, suffer from limitations such as lack of specificity, high costs, lengthy operation times, and the need for skilled personnel [25], [26]. However, surface plasmon resonance-based MTM sensors indeed offer several advantages over traditional methods for cancer cell detection. Their high precision, label-free detection, real-time measurement capabilities, and minimal sample requirement make them promising candidates for improving cancer diagnostics. Recently, a number of research works reported MTM-based sensors in THz range for cancer cell detection [14], [15], [27], [28], [29], [30], [31], [32], [33], [34], [35], [36], [37], [38], in addition to sensors for various other biodetection applications [16], [17], [18], [19], [20], [21], [22], [39], [40], [41], [42], [43], [44], [45], [46], [47]. These reported biosensors for cancer detection are mostly graphene-based [14], [27], [29], [30], while water-based THz MTM absorbers [15] are also presented. Likewise, several ring-based resonator structures [27], [33], [35], [36], [38] for MTM THz sensors are proposed for cancer cell detection.

TABLE I
COMPLETE LIST OF THE VARIABLES THAT HAVE BEEN ADJUSTED FOR THE RECOMMENDED SENSOR

Parameter	Value (μm)	Parameter	Value (μm)
A	49	J	11.6
B	58	K	10
C	10.25	L	55
D	39.3	M	150
E	21.8	N	150
F	20.5	Aluminum (Al) thick	0.2
G	49	Polyimide thick (T1)	10
H	75.8	Coverslip thick (T2)	4
I	30	HeLa Cells thick (T3)	8

This research presents a novel MTM-based compact multiband biosensor for early stage cervical cancer detection, operating from 0 to 6 THz. The sensor features a patterned aluminum structure on a polyimide substrate, optimized for near-perfect absorption. Using full-wave EM simulations, the design process examines absorption characteristics and material effects. The sensor's efficacy is demonstrated with a microwave imaging (MWI) system, distinguishing between healthy and cancerous tissue. Extensive benchmarking against state-of-the-art sensors shows superior performance in absorbance levels and bandwidth, enhancing cancer detection sensitivity.

II. LAYOUT OF THE MODEL'S UNIT CELL AND INCIDENT FIELD CONFIGURATION

The effective conversion of applied energy into absorption is possible due to the unique MTM-inspired structure, as shown in Fig. 1. Perfect absorbers effectively decrease the reflection of incoming energy by absorbing the majority of it. In addition, the design of the MTM minimizes destructive interference, which further enhances absorption and weakens transmitted waves. The absorber is built using a commercial full-wave finite integration technique (FIT) that relies on a high-frequency EM solver. This allows for the study of MTMs across different frequency ranges and limits. Scientists have used numerical analysis to investigate structures such as perfect electric and magnetic conductors (PEC and PMC), unit cells, periodic arrays, and empty space. Fig. 1(a) shows a first resonator and Fig. 1(b) shows a second resonator, respectively. The proposed design shown in Fig. 1(c) represents a creation based upon a combination of first and second resonators. The overall size of the structure is 150 × 150 μm. All dimensions of the proposed structure are represented in Table I.

Fig. 2 illustrates the structural configuration and field directions for an MTM perfect absorber designed to function within the THz frequency range of 0–6 THz. Addressing

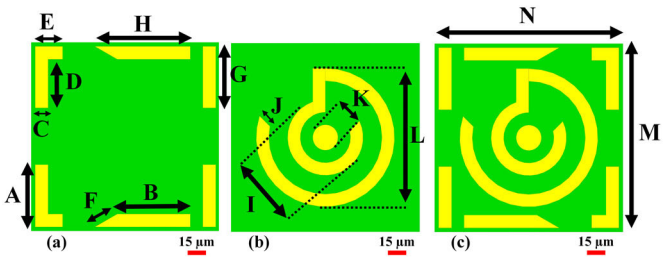

Fig. 1. Suggested structural design for a perfect absorber. (a) First resonators, (b) second resonators, and (c) proposed design.

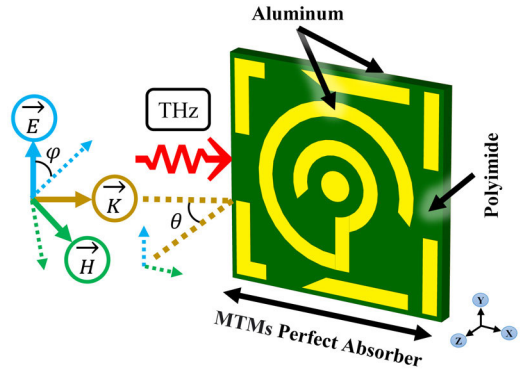

Fig. 2. Configuration of the structural design and the directions of the incident field for a perfect absorber.

the feasibility of high-frequency characterization, the study acknowledges the challenges associated with conventional electronic measurement techniques beyond 100 GHz. However, alternative optical methods, such as THz time-domain spectroscopy (THz-TDS), offer viable solutions for precise characterization within the 0.1 THz to tens of THz range. LTEM and thermal/pyroelectric techniques also present potential alternatives for intensity measurements [48], [49]. These methodologies while requiring further investigation, expand the possibilities for characterizing the proposed THz MTM biosensor. The design comprises an MTM layer, which includes a patterned aluminum structure deposited on a polyimide substrate. This configuration is optimized to achieve near-perfect absorption of incident EM waves over a wide bandwidth. The incident EM wave, depicted by the red arrow, interacts with the absorber surface at specific angles, denoted by θ and φ. The directions of the electric field (E), magnetic field (H), and wave propagation vector (k) are indicated by their respective arrows. These fields are essential for analyzing the absorber's performance, as the interaction between the incident wave and the MTM structure determines the absorption characteristics. The MTM perfect absorber effectively converts the incident EM energy into heat, minimizing reflection and transmission, thereby enhancing the sensing capabilities for applications such as biosensing and spectroscopy in the THz frequency domain.

III. Results and Analysis

In this section, a comparative analysis is conducted covering compact absorber-based sensors tailored for THz operation aiming to obtain an optimized solution for cervical cancer diagnosis. To provide a thorough exploration of various architectural possibilities, this study progressively simulates, and assesses several distinct component designs. These designs are scrutinized based on their absorption spectrum, power distribution, and field density.

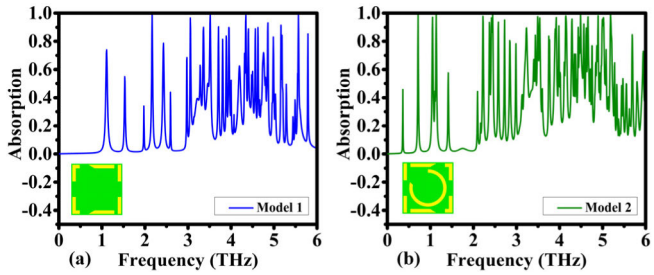

Fig. 3. Showing the different absorption characteristics of two designs. (a) Model 1. (b) Model 2.

A. Absorption Characteristics of Different Designs

The first design under consideration was created from a modified square-shaped split-ring resonator, which is illustrated in Fig. 1(a) and it is sized around 150 μm. To evaluate the performance of the structure, its absorption curve in function of the frequency was computed and the results are shown in Fig. 3(a).

This first model was already an operational design and showed interesting characteristics, as it had several absorption peaks with high absorption coefficients, including regions around 2, 3, 3.5, 4, and 5.5 THz.

A multiband absorber for these upper THz frequencies is of great interest for sensors in several systems, but there is still a desire to have absorption peaks in the frequencies around 1 THz as it presents different propagation behavior in the tissue. Due to that, a new set of designs was evaluated now using the obtained square resonator in conjunction with other structures, initiating with circular path-shaped structures and extending to a mix between circular split rings and bullseye patterned resonators.

The second developed model was evaluated and its results are provided in Fig. 3(b) together with an insert of its physical design. The absorption curve of this design shows great improvement in the frequencies around 1 THz, where at least three peaks clearly obtained very high absorption which partially solves the desired points, but some regions around 3 THz became worse and the very high frequencies over 5 THz are not being well represented too. Trying to achieve these specifications, a circular absorber according to the upper explanations was tried. Its physical constitution is shown in Fig. 1(b) and the resulting absorption spectrum is presented in Fig. 4(a).

The results of this third model were adequate just in the 3–5-THz range and did not show appropriate improvement in the lower or higher frequencies; in this way, the squared resonator was maintained and understood as an important part of the solution, especially for the higher part. In this way, a final model mixed Model 3 and the first model was developed.

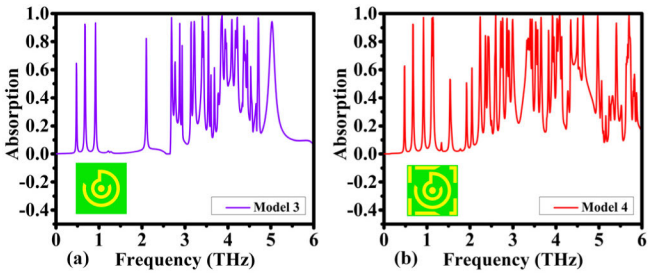

Fig. 4. Different absorption characteristics of the two designs. (a) Model 3. (b) Model 4.

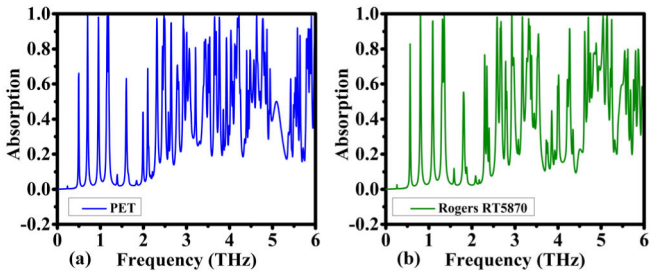

Fig. 5. Absorption spectra for the proposed design under different substrates. (a) PET. (b) Rogers RT 5870.

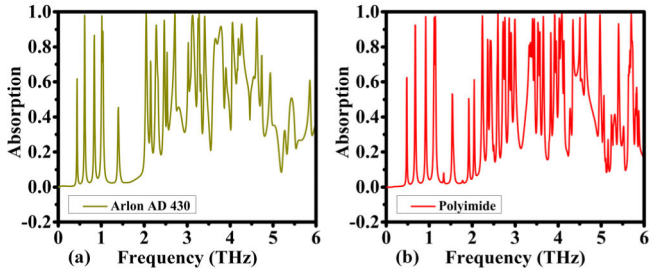

Fig. 6. Absorption spectra for the proposed design under different substrates. (a) Arlon AD 430. (b) Polyimide.

The composition of this last model is shown in Fig. 1(c) and the resulting absorbance spectrum is presented in Fig. 4(b). This model achieved very good results, solving the absence of perfect absorbance peaks near 6 THz while also having several peaks with perfect absorption in the midband and covering the lower 1-THz region. In this way, this design was then chosen as the proposed model for this work and will be further evaluated with respect to its structural properties in the following subsections.

The results of this third model were adequate just in the 3–5-THz range and did not show appropriate improvement in the lower or higher frequencies; in this way, the squared resonator was maintained and understood as an important part of the solution, especially for the higher part. In this way, a final model mixed Model 3 and the first model was developed.

The physical design of this last model is shown in Fig. 1(c) and the resulting absorbance spectrum is presented in Fig. 4(b). This model achieved very good results, solving the absence of perfect absorbance peaks near 6 THz while also having several peaks with perfect absorption in the midband and covering the lower 1-THz region. In this way, this design was then chosen as the proposed model for this work and will be further evaluated with respect to its composing materials in the following section.

The absorption intensity of the peaks is a deliberate feature intended to enhance the sensitivity of a biosensor. This heightened sensitivity is of paramount importance, particularly in practical applications, where accurate discrimination between healthy and cancerous cell samples is essential. The intensified peaks increase the opportunities for interaction with biomolecules, thereby facilitating a more definitive distinction between the two sample types. Multiple peaks correspond to the sensor's multiband functionality, allowing it to detect and differentiate between THz wavelengths for versatile sensing applications, as compared to single-band sensors offering limited applications. The multiband sensor can effectively absorb EM radiations at multiple frequencies, allowing for the operation across a wide frequency range with a comprehensive assessment of sensitivity across all bands. Thus, the multiband configuration enhances the sensitivity of the biosensor at discrete multiple frequency bands.

Although single-band models offer simplicity during fabrication and measurement, however, they suffer from limitations in sensitivity to diverse biomolecular interactions. The preference for the multiband configuration lies in its heightened sensitivity, specificity, and versatility. The multiband approach enables a more thorough and detailed analysis of THz interactions with biological samples, addressing the complexities of biomolecular signatures and minimizing cross-sensitivity, thus establishing it as the preferred choice for advanced biosensing applications.

B. Influence of Substrate and Resonator Material

MTM absorbance characteristics can be very sensitive to its composing materials and aiming to find an adequate material choice, the influence of substrate and resonator material was evaluated, trying to obtain an optimal balance of its ease of use, availability, and resulting characteristics.

The analysis started focusing on the substrate material, where PET and Rogers RT 5870 were evaluated for their absorption characteristics in Fig. 5(a) and (b), respectively. PET produced acceptable results maintaining several near-perfect absorption peaks. On the other hand, the RT 5870 did not work well in high frequencies. Other two materials were also evaluated, the Arlon AD 430 and polyimide in Fig. 6(a) and (b), respectively.

Arlon AD 430 performed even worse than the RT 5870, but polyimide was very successful, being slightly superior to PET, being easy to integrate, and providing good results in both low, middle and high, and high bands. The design was then evaluated with respect to its resonator material, where gold, silver, copper, and aluminum were simulated and its absorption results are presented in Figs. 7(a) and (b) and 8(a) and (b).

The influence of the resonator metal was found to be minor in relation to the changes eventuated in the substrate

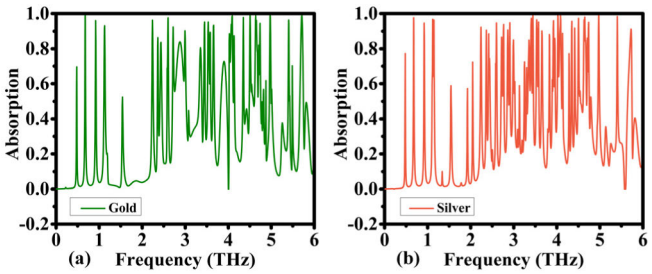

Fig. 7. Absorption spectra for the proposed design under various resonator material conditions. (a) Gold. (b) Silver.

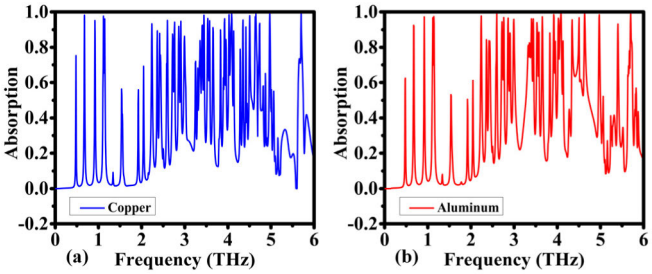

Fig. 8. Absorption spectra for the proposed design under various resonator material conditions. (a) Copper. (b) Aluminum.

material analysis. All the four metal options evaluated worked adequately having several peaks in all ranges well above 0.8. Gold and aluminum were the best metals, but the easiness of fabrication, low cost, higher availability, and better lithography and process integration favor aluminum, which was the final selected material together with the polyimide substrate to form the proposed micro-biosensor. The following subsections evaluates the substrate thickness selection.

C. Effect of Substrate Thickness

The performance of sensors depends on substrate thickness can affect their absorptivity. Research shows that variations in substrate thickness have a direct effect on the level of sensor absorptivity [50]. Sensors' sensitivity and detection capacities can be affected by thicker substrates' effects on their optical characteristics [51]. In addition, in some sensor applications, the thickness of the substrate influences horizontal magnetoresistance, which in turn affects the ability to detect horizontal magnetic fields (H-field) [52]. Substrate design, particularly thickness, is vital for attaining high sensitivity, stabilization, and homogeneity of molecules on the substrate in the context of carbon-based surface-enhanced Raman scattering (SERS) sensors. This has a substantial impact on the sensor's enhancement factor and detection capability [53].

A significant element that profoundly impacts the ability of sensors to absorb and function effectively across various applications is the thickness of the substrate. The investigation illustrated in Figs. 9–12 is focused on exploring the influence of substrate thickness on absorption capacity within a specific frequency range from 0 to 6 THz. Each Figure displays different substrate thicknesses and their respective responses, providing insight into how different thicknesses impact the

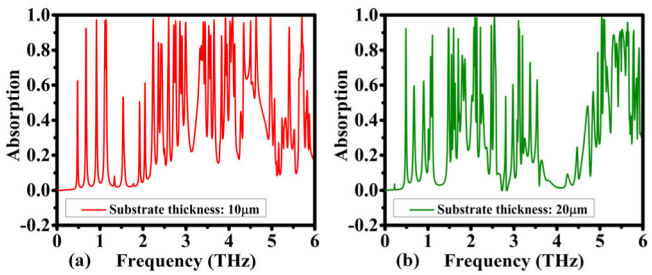

Fig. 9. Investigating the effect of the proposed substrate thickness on the ability to absorb (a) substrate thickness 10 μm and (b) substrate thickness 20 μm.

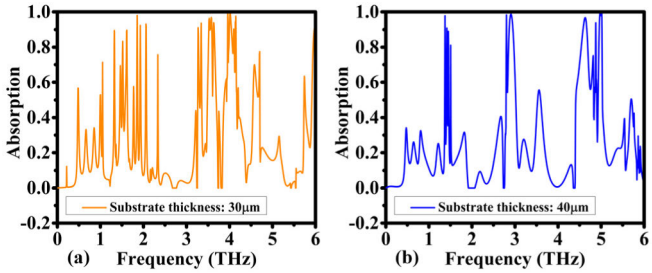

Fig. 10. Investigating the effect of the proposed substrate thickness on the ability to absorb (a) substrate thickness 30 μm and (b) substrate thickness 40 μm.

capacity to absorb EM waves. An initial observation from Fig. 9(a) and (b) with substrate thicknesses of 10 and 20 μm reveals a favorable response throughout the frequency spectrum. This indicates that relatively thinner substrates exhibit favorable absorption properties in the specified frequency range. A good response implies efficient interaction between EM waves and the substrate, resulting in effective absorption.

The influence of different substrate thicknesses on absorption efficiency within specific frequency ranges is illustrated in Fig. 10. When the substrate thickness is 30 μm in Fig. 10(a), absorption rates exceeding 80% are noticed between 1–2 and 3–4 THz. Conversely, in Fig. 10(b) with a thicker substrate of 40 μm, notably improved absorption performance is noticed above 90%, especially at 1.5 THz, 3 THz, and ranging from 4.5 to 5.2 THz. These findings indicate a relationship between substrate thickness and absorption capacity, with thicker substrates demonstrating absorption across the 0–6-THz frequency bands.

Fig. 11 illustrates the impact of modifying substrate thickness on absorption efficiency, with a thickness of 50 and 60 μm. In Fig. 11(a), absorption levels exceed 85% within frequency bands ranging from 0.8 to 1.5 THz, 2 to 3 THz, and at 4.5 and 5.5 THz. In contrast, Fig. 11(b) demonstrates superior absorption, exceeding 90% at 1, 1.5–2.5, 3–3.5, 4.5–5, and 5.5–6 THz. Thicker substrates enhance absorption performance, potentially by altering EM field distribution and impedance matching. These results reveal the importance of optimizing substrate thickness for specific frequency ranges essential for applications, such as sensing and communication. The study emphasizes the complex link between substrate

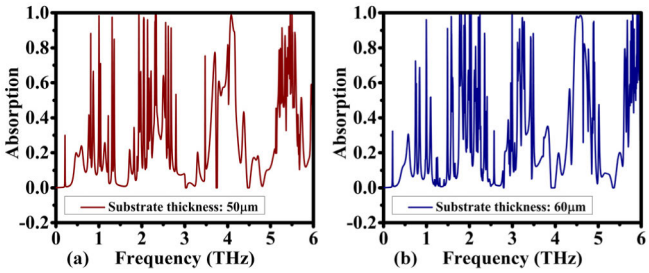

Fig. 11. Investigating the effect of the proposed substrate thickness on the ability to absorb (a) substrate thickness 50 μm and (b) substrate thickness 60 μm.

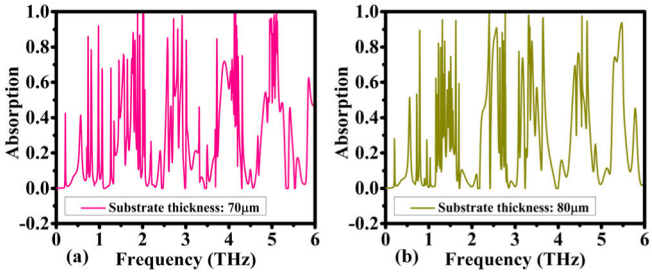

Fig. 12. Investigating the effect of the proposed substrate thickness on the ability to absorb (a) substrate thickness 70 μm and (b) substrate thickness 80 μm.

thickness and absorption capacity. Thicker substrates provide more material for EM waves to interact with, likely leading to increased absorption.

Finally, Fig. 12 further illustrates comparative study on how the thickness of a substrate impacts its ability to absorb at various frequencies in a range from 0 to 6 THz. In Fig. 12(a) where the substrate is 70 μm thick, absorption levels surpass 80% over a range of frequencies from 1 to 6 THz, showing peaks at 1, 2, 2.5–3, 4, and 5 THz, respectively. On the other hand, in Fig. 12(b) with a substrate thickness of 80 μm, absorption levels above 80% are observed within a narrower frequency span, notably at frequencies 0.5, 1–2, 3, 3.5, 4.5, and 5.5 THz, respectively. These results suggest that the thickness of the substrate significantly affects its absorption properties. Thinner substrates display wider absorption peaks spanning a broader frequency range, while thicker substrates exhibit narrower absorption peaks concentrated at specific frequencies. This understanding is crucial for optimizing substrate design for various applications, such as sensors, communication devices, and EM shielding.

D. EM Properties and Simulation Responses

Fig. 13 illustrates the impact of permeability (μ) and permittivity (ε) on the absorptive properties of MTMs and their interaction with EM radiation. The analysis of these components is crucial for optimizing absorption efficiency and sensitivity in detecting biological analytes. The real parts influence wave propagation and absorption, while the imaginary parts indicate the dissipative nature of the material. Furthermore, Fig. 13 demonstrates the real and imaginary

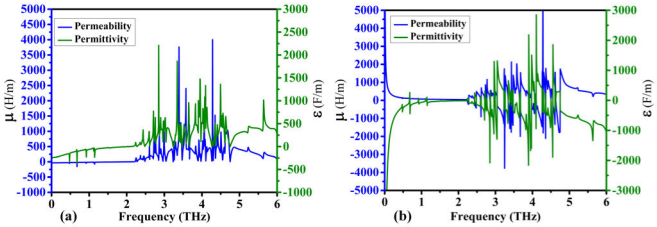

Fig. 13. (a) Real parts and (b) imaginary parts of permeability μ and permittivity ε of the proposed absorber.

components of the permeability (μ) and permittivity (ε) of the recommended absorber. Fig. 13(a) emphasizes the real parts of permeability (μ) and permittivity (ε), which signify the material's capacity to support H-fields and store electrical energy, respectively. These characteristics are vital for efficiently absorbing EM waves. A high real part of permeability indicates a strong magnetic response, while a significant real part of permittivity suggests the ability to store electrical energy, facilitating absorption [54]. Fig. 13(b) presents the imaginary parts of permeability (μ) and permittivity (ε), which demonstrate the dissipative losses in the material due to the absorption of EM energy. A high imaginary part of permeability demonstrates the effective absorption of H-field energy, while a notable imaginary part of permittivity indicates the absorption of electrical energy. These elements are crucial for ensuring the successful attenuation of incident EM waves within the material, preventing reflection or transmission [55], [56]. In addition, Fig. 13 provides insights into the interaction of the material with THz waves by examining permeability (μ) and permittivity (ε) across the frequency range of 0–6 THz. Through the examination of the real and imaginary parts of μ and ε, researchers can better understand wave propagation and absorption characteristics necessary for achieving multiband absorption tailored to specific biomolecules.

The MTM response in this article, including permeability and permittivity from 1 to 6 THz, is justified despite the unit cell periodicity of 150 μm. MTM qualities are generally specified by unit cells smaller than the wavelength; however, in the THz region, EM waves may interact with subwavelength structures to yield effective medium parameters that are suggestive of MTMs. Many resonance peaks detected within the frequency range of interest are compatible with MTM behavior caused by complicated EM interactions inside the structure. At these scales, the effective medium approximation holds true, enabling the structure to display MTM properties such as negative permeability or permittivity at certain frequencies. As a result, the periodicity limitation does not prevent the structure from being classified as an MTM within the given frequency range, allowing for an accurate interpretation of the biosensor's performance.

Fig. 14 provides a thorough evaluation of biosensor performance by analyzing impedance (z) and the reflection coefficient (S_{11}). The variations in impedance allow for the examination of the biosensor's ability to interact with biological samples and detect changes in their dielectric properties.

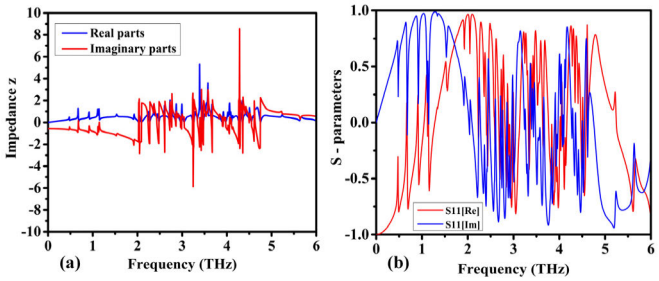

Fig. 14. Simulated responses of parameters of the proposed model (a) impedance z and (b) S_{11} real and imaginary parts.

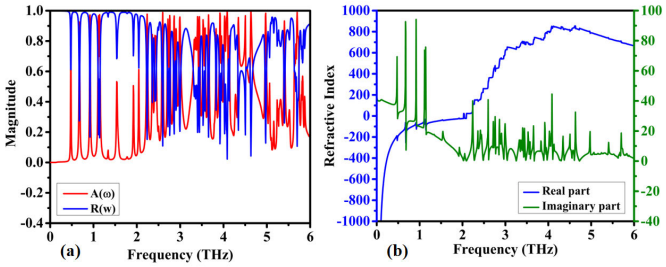

Fig. 15. Simulated responses of parameters for the proposed model (a) reflection and absorption spectra of the absorber and (b) real and imaginary parts of the refractive index.

On the other hand, the analysis of S_{11} helps to understand the biosensor's reflectance characteristics and its interaction with external stimuli. This comprehensive understanding is crucial for refining biosensor design, enhancing sensitivity, and optimizing performance for various biomedical sensing applications. Fig. 14 depicts the simulated responses of parameters in the proposed framework, with a particular focus on impedance (z) and the real and imaginary components of the S_{11} parameter. These elements play a significant role in understanding the behavior of electronic circuits, particularly in radio frequency (RF) and microwave engineering. Fig. 14(a) shows impedance (z) measures the resistance to alternating current flow in a circuit. The illustrated responses present how the circuit reacts to various frequencies. Alterations in impedance can changes signal in the circuit's behaviors such as its resonance frequency or bandwidth. Understanding impedance services researcher in designing circuits that can efficiently transmit or receive signals without loss. In Fig. 14(b), the S_{11} parameter, depicted through its real and imaginary parts, is widely utilized in RF and microwave engineering to elucidate the reflection coefficient of a circuit or device. The real part denotes the reflection's magnitude, while the imaginary part signifies the phase shift resulting from the reflection. By examining both aspects of the S_{11} parameter, researcher can evaluate how effectively a circuit conveys energy from a source to a load or the amount of energy reflected due to impedance mismatches [57]. In addition, Fig. 14 evaluates absorption efficiency by examining impedance (Z) and the S_{11} parameter. A close-to-zero impedance and a magnitude of S_{11} close to 1 (0 dB) at desired absorption frequencies indicate efficient absorption of THz waves, which is essential for bio-sensing applications. These figures directly contribute to the optimization of MTM design and the prediction of sensor performance, ultimately facilitating successful biosensing within the THz range.

The proposed biosensor acts as a perfect absorber and exhibits remarkable absorption properties in the THz spectrum, specifically within the range of 0–6 THz. Its performance is distinguished by multiple sharp absorption peaks, each exceeding 95% at specific frequencies within this range. This exceptional behavior is demonstrated through the absorption spectrum, which displays several distinct peaks, as shown in Fig. 15(a). Correspondingly, the reflection spectrum shows matching dips at these same frequencies. This inverse relationship between absorption peaks and reflection dips indicates that the absorber is highly efficient at absorbing THz radiation at these target frequencies while minimizing reflection losses. The refractive index of MTMs plays a vital role in biosensing applications, particularly for medical diagnostics, such as cervical cancer detection. To validate the proposed structure, it is essential to demonstrate that it possesses a negative refractive index and negative permittivity properties.

Fig. 13 shows the real and imaginary parts of permeability (μ) and permittivity (ε), which exhibit significant fluctuations and dip below zero at certain frequencies. This confirms the presence of negative refractive index properties, characteristic of MTMs, enhancing sensitivity and specificity for biosensing. Fig. 15(a) presents the reflection and absorption spectra, highlighting high absorption peaks corresponding to frequencies with negative permittivity and permeability from Fig. 13. In particular, significant absorption occurs around 2–6 THz, aligning with negative values. Fig. 15(b) shows the real and imaginary parts of the refractive index, further validating the MTM properties. The negative values at specific frequencies indicate unconventional EM wave manipulation, supporting high sensitivity and specificity. The figures demonstrate that negative permeability and permittivity (see Fig. 13) translate into practical outcomes, such as reduced reflection and increased absorption (see Fig. 15), affirming the sensor's MTM functionality. These properties ensure the sensor's capability for sensitive detection of early stage cervical cancer.

E. MTM Structure Field Distributions

Analyzing the electric field (E-field) in THz MTM perfect absorber biosensors for cervical cancer detection is vital. The real part [Re(E)] indicates E-field magnitude and direction, especially the Ez-field along the z-axis, revealing energy storage and directionality. High Re(E) values in MTM layers show strong THz wave interaction. The imaginary part [Im(E)] reflects energy dissipation due to material properties, crucial for perfect absorption. Analyzing Ez-field with CST Studio Suite aids visualization of real and imaginary components at various frequencies, correlating with absorption characteristics (e.g., S_{11} parameter). This analysis, combined with biomarker studies, strengthens biosensor efficacy in early cancer detection at THz frequencies.

Fig. 16 displays the field distribution of an MTM perfect absorber designed for use within the 0–6-THz frequency range. The MTM absorber, characterized by a multiband response with approximately 18 resonance points, exhibits distinct

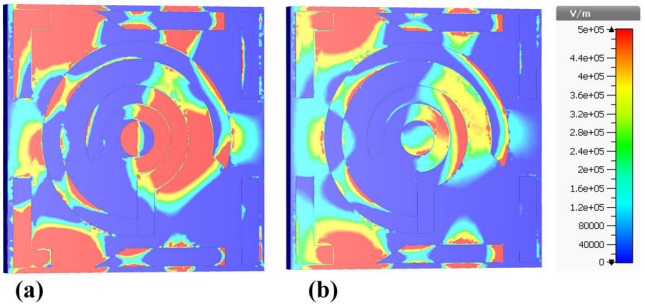

Fig. 16. Distributions of the MTM structure field are shown on a color map. (a) *Ez*-field real part. (b) *Ez*-field imaginary part.

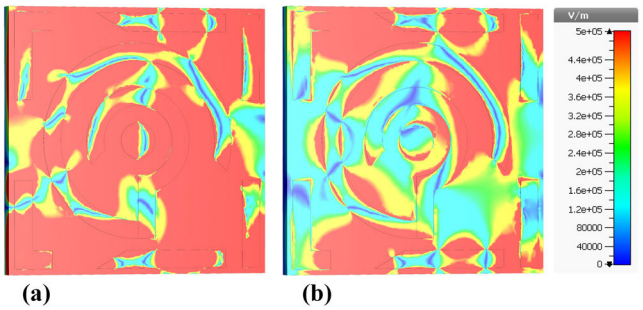

Fig. 17. Distributions of the MTM structure field are shown on a color map. (a) /*E*/-field real part. (b) /*E*/-field imaginary part.

peaks in its absorption spectrum. Fig. 16 illustrates the *E*-field (*Ez*) distributions of the MTM structure, with Fig. 16(a) representing the real part and Fig. 16(b) representing the imaginary part of the *Ez*-field component.

In Fig. 16(a), the real part of the *Ez*-field distribution is shown in a color map, where different colors represent the intensity of the *E*-field at various points on the MTM surface. The scale on the right, marked in V/m, indicates the *E*-field strength, ranging from low (blue) to high (red) values. The areas with higher field intensities correspond to the regions where the MTM structure interacts most effectively with the incident EM waves, leading to enhanced absorption.

Fig. 16(b) presents the imaginary part of the *Ez*-field distribution, which is critical for understanding the phase behavior of the *E*-field across the MTM surface. Similar to the real part, the color map indicates the field strength, with variations in the imaginary component reflecting the reactive properties of the MTM. The combination of these field distributions provides insights into the resonance behavior and efficiency of the MTM absorber, highlighting how the structure can effectively manipulate and absorb incident THz waves across multiple frequencies. This detailed analysis of the field distributions is essential for optimizing the design and enhancing the performance of the MTM absorber for applications in sensing and imaging.

Fig. 17 illustrates the *E*-field distributions of a THz MTM biosensor designed for early cervical cancer detection, separated into the real [see Fig. 17(a)] and imaginary [see Fig. 17(b)] components of the *E*-field (/*E*/-field). The MTM structure exhibits 18 distinct sharp resonance peaks within the 0–6-THz range, demonstrating the sensor's high sensitivity and multiband capability essential for biosensing. These multiple peaks enable detailed tissue characterization, enhancing the detection of subtle changes associated with early stage cancer while also improving specificity and robustness for reliable diagnosis. The *E*-field density is color-mapped, ranging from 0 to 5×10^5 V/m.

In Fig. 17(a), the real part of the /*E*/-field [Re(*E*)] demonstrates the magnitude and direction of the *E*-field within the MTM structure. High values, depicted in red, are predominantly observed within the aluminum resonators, signifying regions of strong interaction with THz waves and efficient absorption. This interaction is crucial for enhancing the biosensor's sensitivity to the presence of biomarkers indicative of cervical cancer. In contrast, Fig. 17(b) shows the imaginary part of the /*E*/-field [Im(*E*)], highlighting the energy storage and dissipation within the MTM. Positive values, indicated by varying colors from yellow to red, suggest areas where energy absorption is efficient, aligning with the design goal of achieving perfect absorption for optimal sensor performance.

The comprehensive analysis of the /*E*/-field components using EM simulation tools, such as CST Studio Suite allows for detailed visualization and optimization of the biosensor's performance. By identifying regions with high real part values (indicating strong field intensity) and positive imaginary part values (indicating efficient absorption), researchers can fine-tune the sensor design to maximize its effectiveness in detecting early stage cervical cancer. This approach ensures that the biosensor can accurately and reliably identify the presence of cancer biomarkers, thereby facilitating early diagnosis and improving patient outcomes.

In the context of our biosensor designed for early cancer detection, understanding the *H*-field's division into real and imaginary parts (*Hz*-field) is crucial. The real part of the *Hz*-field (*Hz*-real) is associated with the biosensor's resonant behavior and absorption properties, which directly impact its performance. Conversely, the imaginary part (*Hz*-imaginary) reflects energy dissipation within the biosensor due to losses, such as absorption and scattering, influencing sensitivity, and signal-to-noise ratio.

Analyzing the Hz-field for both real and imaginary parts involves utilizing software, such as CST Studio, which employs numerical methods, such as the finite element method (FEM) or finite-difference time-domain (FDTD) simulations. These simulations calculate the distribution of the *Hz*-field within the biosensor structure, providing insights into its behavior in the THz range (0–6 THz). CST Studio generates visualizations depicting the magnitude and direction of the *Hz*-field across the biosensor, with blue representing minimum intensity and red indicating maximum intensity, typically ranging from 0 to 100 A/m.

The images produced by CST Studio offer qualitative insights into how the *Hz*-field interacts within the biosensor at specific frequencies. Areas with stronger red hues denote regions of higher *H*-field intensity, providing valuable information for optimizing the biosensor's performance. However, for a comprehensive evaluation, it's essential to correlate these *Hz*-field characteristics, particularly the real and imaginary

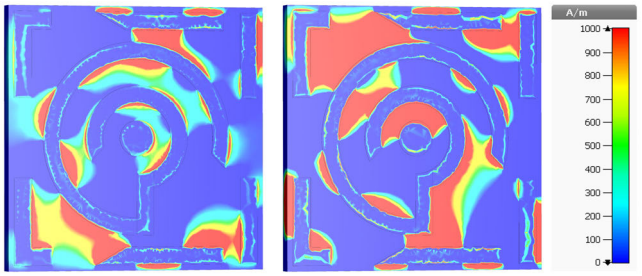

Fig. 18. Distributions of the MTM structure field are shown on a color map. (a) *Hz*-field real part. (b) *Hz*-field imaginary part.

parts, with overall absorption efficiency and resonance behavior, especially in the context of early cervical cancer detection.

Fig. 18 presents the H-field (Hz-field) distributions of an MTM-based biosensor tailored for multiband THz sensing in the 0–6-THz range, aiming at early cervical cancer detection, with H-field intensity varying from 0 to 1000 A/m. The real and imaginary parts of the Hz-field distribution are, respectively, illustrated in Fig. 18(a) and (b), playing pivotal roles in understanding the biosensor's behavior and performance. Analyzing these distributions using computational techniques allows for a detailed scientific explanation, involving calculations of field patterns, resonance frequencies, absorption spectra, and other relevant parameters, based on the MTM structure's interaction with THz waves. The color maps in Fig. 18 provide visual representations of the H-field distributions within the biosensor's MTM structure, with a color scale indicating intensity ranging from blue (0 A/m) to red (1000 A/m). Fig. 18(a) showcases a complex pattern of the H-field, with varying intensities denoted by colors, suggesting concentrated regions within the MTM structure possibly associated with resonant behavior at specific THz frequencies. In Fig. 18(b), the imaginary part of the Hz-field distribution exhibits a similar intricate pattern but with differences in intensity distribution, reflecting energy loss due to absorption or scattering and indicating the MTM's interaction with THz waves in terms of energy dissipation. The biosensor's design, as inferred from these images, is likely optimized to enhance sensitivity and specificity for early cervical cancer detection by capitalizing on the unique interactions between THz waves and the MTM structure. Its multiband nature suggests the capability to detect multiple resonant frequencies, potentially corresponding to different cancer biomarkers. Understanding both the real and imaginary parts of the Hz-field distributions is critical for refining the biosensor's design, considering factors such as MTM geometry, composition, and their interactions with THz waves, all crucial for optimal sensor performance.

Analyzing the real and imaginary part's absolute value of the H-field ($|H|$-field) in the context of our biosensor design is crucial for understanding its performance, especially in THz frequencies. In MTM-based biosensors, the real part absolute value of the H-field $|H$-real| relates to the distribution and strength of the H-field within the device. It characterizes the resonant behavior and absorption properties of the biosensor. A strong correlation between the real part of the H-field and biosensor performance indicates efficient absorption and detection of cancer biomarkers.

Conversely, the imaginary part absolute value of the H-field $|H$-imaginary| represents the dissipation of energy within the biosensor due to losses, such as absorption and scattering. Higher values of $|H$-imaginary| signify increased energy loss, which can impact the sensitivity and signal-to-noise ratio of the biosensor. Monitoring the imaginary part of the H-field is essential for optimizing the device's performance and minimizing signal degradation.

CST Studio Suite, a robust EM simulation software, is utilized for analyzing EM field behavior within intricate structures, such as the described biosensor. In assessing the absolute value of the H-field ($|H|$-field) for real and imaginary components, CST Studio Suite employs numerical methodologies, particularly FEM or FDTD simulations. Initially, the software generates a mesh to discretize the simulation domain, encompassing the biosensor and its environment, facilitating the numerical solution of Maxwell's equations. Subsequently, parameters such as frequency range, material properties, and excitation sources are specified in the solver setup phase. Following this, CST Studio Suite executes numerical simulations based on the defined parameters, iteratively solving Maxwell's equations to determine EM field distributions within the biosensor. Upon completion, the software produces visualizations of EM fields, including the $|H|$-field, representing its magnitude and spatial distribution. These visualizations, outputted in formats such as 2-D plots or color maps, aid researchers in interpreting H-field behavior within the biosensor, facilitating optimization for efficient cancer biomarker detection. By visualizing $|H$-real| and $|H$-imaginary|, researchers can assess the resonant behavior, absorption efficiency, and losses of the biosensor across different frequencies in the THz range.

Fig. 19 depicts the H-field distribution within a THz biosensor using color maps (0–2000 A/m, blue–red scale). Fig. 19(a) shows the real part ($|H$-real|), a complex pattern with swirling colors indicating the H-field intensity. Red and yellow areas represent high intensity, while blue signifies low. This part relates to energy storage and offers insights into the biosensor's resonance behavior. Fig. 19(b) shows the imaginary part ($|H$-imaginary|), also displaying a complex pattern but dominated by red, indicating higher overall intensity. This part reflects energy dissipation within the MTM due to absorption and scattering. The color distribution reveals how the biosensor interacts with THz waves. The intricate patterns suggest the MTM is designed to create localized enhancements of the H-field, potentially improving sensitivity and specificity for detecting cervical cancer biomarkers. Analyzing both parts of the H-field distribution allows researchers to refine the biosensor design for optimal performance at specific THz frequencies.

Fig. 20 illustrates the surface current distribution on an MTM structure tailored for a THz-range biosensor aimed at early cervical cancer detection. The color scale indicates current intensity from 0 A/m (blue) to 1000 A/m (red). In Fig. 20(a), the real part of the surface current distribution is depicted, showcasing arrows representing the

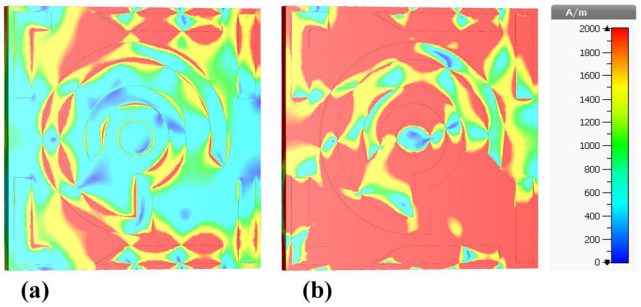

Fig. 19. Distributions of the MTM structure field are shown on a color map. (a) /*H*/-field real part. (b) /*H*/-field imaginary part.

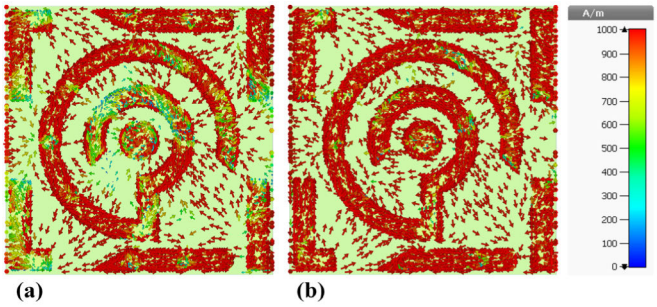

Fig. 20. Recommended MTM's surface current distribution. (a) Real part. (b) Imaginary part.

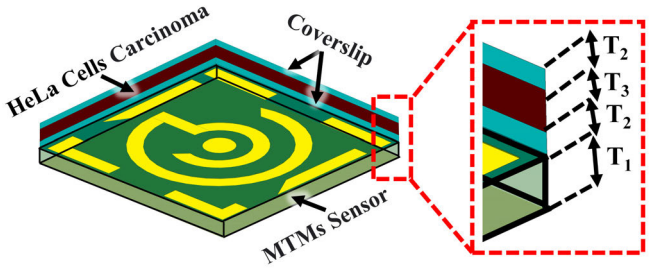

Fig. 21. Suggested biosensor investigates the absorption coefficient in both healthy cervical and cervical cancer.

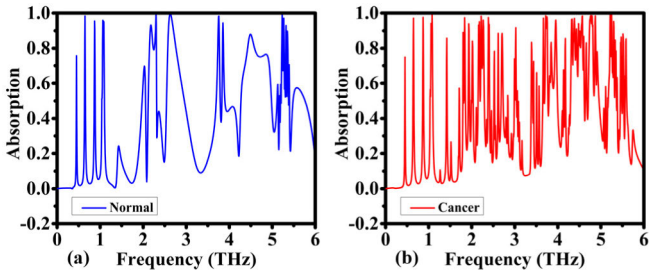

Fig. 22. Proposed biosensor detects absorption coefficients in the frequency range from 0 to 6 THz. (a) Normal cervical. (b) Cervical cancer.

current direction and magnitude across the MTM's surface. Red arrows highlight areas of intense current, indicating strong resonant interactions with THz waves and suggesting frequency-sensitive biomarker detection. Fig. 20(b) displays the imaginary part of the surface current distribution, with red arrows denoting higher intensity. This part reflects energy dissipation within the MTM, including inherent resistance and other dissipative effects, crucial for biosensor sensitivity and specificity. The biosensor's design, evident in these images, is pivotal for performance, revealing its interaction with THz waves to detect cervical cancer biomarkers. Analyzing both parts of the surface current allows researchers to refine the biosensor's design for optimal detection capabilities across multiple THz frequencies. The ultimate objective is to develop a biosensor capable of early stage cervical cancer detection by selectively identifying molecular signatures, potentially improving patient outcomes through timely diagnosis and treatment.

IV. Diagnosis of Cervical Cancer

To gain more details and rigorously investigate the performance of the healthy cervical and cervical cancer sensor, here, we used numerical analysis to simulate the structure. The 3-D shape in Fig. 21 displays the MTMs' configuration of the structure. Here, the structural parameters are set as four layers including T1, T2, T3, and T2 so that the absorption spectrum is used for detection in resonance wavelength near the THz range. As can be seen, a coverslip is placed on the structure to enhance of light–matter interaction leading to higher-to-higher absorption. Besides, to obtain the same results, HeLa cell carcinoma is defined. Then, the footprint of the structure is in agreement with the experimental point of view corresponding to the multiresonance modes.

HeLa cells, commonly used in cancer research, have a refractive index of around 1.38, with specific values of 1.392 for malignant tissue and 1.368 for healthy cervical tissue [58], [59], [60], [61], [62], [63]. Culturing HeLa cells requires a nutrient-rich medium rather than water, as water alone would cause cell death due to osmotic stress. The presence of HeLa cells influences the sensor response by altering the dielectric environment, leading to shifts in resonance peaks. This frequency dependency results in different optical properties and absorption bands. In addition, HeLa cells' unique behaviors and genetic variations over time can impact the reproducibility of experimental results, necessitating careful consideration to ensure data accuracy.

Cervical cancer is a type of cancer that occurs in the cells of the cervix, which is the lower part of the uterus that connects to the vagina. Diagnosis of cervical cancer typically involves a combination of medical history, physical examination, Pap smear, HPV testing, and biopsy. During a Pap smear, cells are collected from the cervix and examined under a microscope to look for any abnormalities. If abnormal cells are found, further testing may be done, including HPV testing to check for the presence of the human papillomavirus, which is a known risk factor for cervical cancer.

If abnormal cells are detected, a biopsy is usually performed to confirm the diagnosis of cervical cancer. A tissue sample is taken from the cervix and examined by a pathologist to determine if cancer is present.

To compare the absorption properties of the proposed sensor based on the cavity with a structure based on the circular cavity, the absorption spectrum in the normal case (blue curve) and in the detection case (red curve) is also shown in

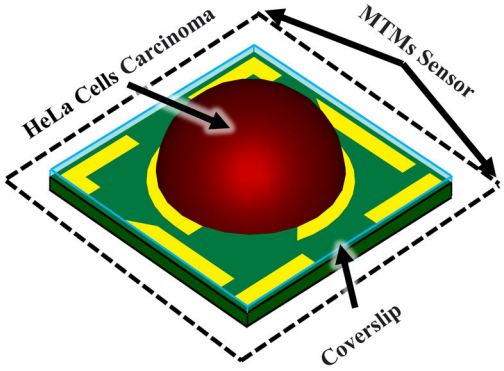

Fig. 23. Diagnosis of cervical cancer using the MWI technique.

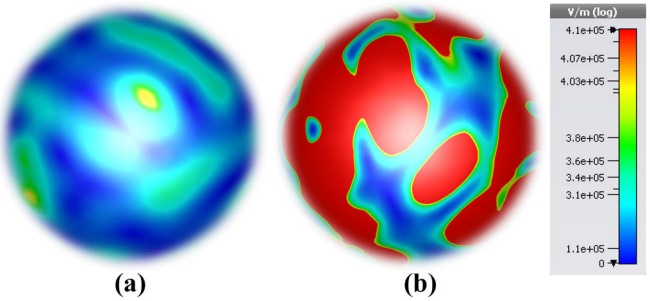

Fig. 24. *E*-field MWI technique results. (a) Normal cervical. (b) Cervical cancer.

Fig. 22(a) and (b), respectively. The corresponding resonance frequency occurs from 0 to 6 THz, with absorption values of approximately 1 and FWHM values of about 0.5 THz around 2–3 THz.

MWI is a developed method with noteworthy potential to supplement recognized imaging methods to enhance biomaterial and cancer detection. To date, numerical simulations have been applied to analyze the different MWI methods, but some methods have been conducted. To cope with this issue, here numerical simulation with MWI technique is a reliable scenario that can improve absorption which leads to higher sensitivity. The same structure is shown in Fig. 23.

To further investigate the performance of the above-mentioned structure, we have also inspected the *E*-field MWI technique in two cases: 1) the left panel (normal case [see Fig. 24(a)]) and 2) the right panel (cancer case [see Fig. 24(b)]). The *E*-field for these cases is tuned from 0 to $4.1e^{+05}$ V/m. As can be seen by considering the cancer case [see Fig. 24(b)] high light–matter interaction is occurred.

H-field MWI is a technique used in nondestructive testing and imaging to detect and visualize hidden defects or anomalies in materials. It works by transmitting microwave signals and measuring the *H*-field response generated by interactions with the material. This technique can be used for various applications such as quality control in manufacturing, inspection of composite materials, and medical imaging.

In contrast, in order to study the relationship between the two cases with *H*-filed considering the MWI technique, the numerical results are calculated. As can be seen in

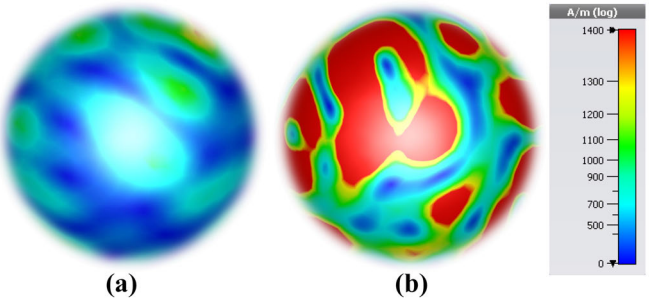

Fig. 25. *H*-field MWI technique results. (a) Normal cervical. (b) Cervical cancer.

TABLE II
BIOSENSING PERFORMANCE COMPARISONS OF VARIOUS SENSOR APPLICATIONS BASED ON MTM

Ref.	Year Published	FOM (RIU−1)	Q	S (THz/RIU)	Bio-application
[16]	2014	0.1216	5.58	0.02432	detection of Penicillia
[17]	2017	-	-	0.0242, 0.02438	detection of Virus
[18]	2020	-	-	0. 960	Biosensor, Collagen
[19]	2020	1.88	6.6	0.285	sensor
[27]	2021	-	10.64	1.65	Cancer detection
[20]	2021	-	-	0. 2833	Polystyrene particle
[38]	2021	-	-	0.074	Cervical cancer
[29]	2022	3.86	13	0.207	Cancer detection
[22]	2022	0.166	-	1.06	detection of avian influenza virus
[64]	2022	-	-	0.068	Hepatocellular carcinoma
[21]	2022	1.81, 1.57	8.21, 6.05	0. 203	sensor
[14]	2022	2.75	2.43	1.21	Cancer Diagnosi, Biosensor
[65]	2023	-	11	0.278	Bovin serum albumin protein
[66]	2023	-	82	0.495	Cancer detection
[28]	2023	0.86, 1.15	12.8, 13.5	0.0515, 0.076	Non-Melanoma Skin Cancer Diagnostics
This work	-	3525838	45.056	236640	Cervical cancer

Fig. 25(a) and (b), *H*-field is tuned from 0 to 1400 A/m. The main result is seen in absorption and high interaction.

V. FUTURE PERSPECTIVE

Early stage detection of various cancers, including colon cancer, blood cancer, adrenal gland cancer (PC-12), breast cancer, and nonmelanoma skin cancer, can be achieved through the use of THz EM (EM) wave imaging biosensors.

VI. BENCHMARKING

This article introduces a cutting-edge biosensor engineered with an MTM perfect absorber, tailored for the early detection of cervical cancer. Operating within the THz range of 0–6 THz, the biosensor is multiband, featuring over 18 resonance peaks. The performance metrics of this biosensor are exceptional when compared to previously developed biosensors, as evidenced by its high sensitivity of 236 640 THz/RIU, high quality factor of 45.056, and an impressive figure of merit (FOM) of 3 525 838 RIU^{-1}, detailed in Table II.

TABLE III
COMPARISON BETWEEN THE THz BAND STUDY ON PERFECT MTMs AND THE RECOMMENDED BIOSENSOR

Ref.	Material substrate	Frequency operating THz	Absorptivity	Techniques used	Application
[39]	SiO2	7-9.5	0.98	Au/SiO2/ Graphene	Multi-Frequency Broadband and Ultra-Broadband
[40]	silicon dioxide	1.5-1.7	0.972, 0.991	Gold/silicon dioxide/ Gold	biosensor for detecting coronaviruses
[14]	SiO2	0.5-2.5	-	SiO2/Graphene	Breast cancer detection
[41]	SiO2	2−6	0.99	graphene/Au/SiO2/Au	Refractive index sensor
[15]	Glass	0-0.37	0.998	Glass/InSb/MgF2/InSb	Colon Cancer Detection
[42]	photonic crystal plate	1−3	0.97, 0.98, 0.99	bulk Dirac semimetal/photonic crystal/Au	Narrowband perfect absorber
[43]	dielectric layer	1−3	0.99, 0.99	Au/dielectric layer/Au	Sensor
[44]	PET	0-3	0.99, 0.80, 0.95	PET/FSS/UV glue/ Graphene	Multifunctional Tunable Terahertz
[45]	Teflon	0.7-5	>0.96	Ion gel/Graphene/Teflon/Gold	polarization-sensitive
[46]	Topas spacer	0.5−4.5	0.99, 0.98, 0.99	graphene/Topas/Au	Ultra-Broadband Absorber
[47]	dielectric Teflon	1−2.2	0.99	Au/dielectric Teflon/Au	Sensor
This work	Polyimide	0−6	Ten peaks: > 0.97 Six peaks: > 0.98 Two peaks: > 0.998	Al/ Polyimide /Al	Cervical cancer, Microwave Imaging and Biosensor

Further demonstrating its superiority, the proposed biosensor achieves remarkable absorbance levels across its resonance peaks: ten peaks exceed 97% absorbance, six exceed 98%, and two surpass 99.8%, within a 6-THz operating bandwidth, as summarized in Table III. This competitive performance highlights the proposed biosensor's potential for significant advancements in early stage cervical cancer detection, outperforming many existing biosensors in both sensitivity and efficiency.

VII. CONCLUSION

This study focused on developing a novel multiband biosensor structure for the early stage detection of cervical cancer. The sensor is an MTM-based design intended to operate in the low-THz range, from 0 to 6 THz. It features an MTM layer implemented as a patterned aluminum structure placed on a polyimide substrate. The design process was meticulous, aiming to achieve near-perfect absorption of incoming EM waves across the entire operating frequency range. Full-wave EM simulation tools were used to accurately evaluate the system properties. This article provides a detailed explanation of the intermediate steps in the sensor's topology development along with an EM-based investigation of the absorption characteristics. Additional studies examined the effects of the substrate material and thickness and the resonator material. An MWI system incorporating the device was analyzed to demonstrate the proposed sensor's utility for early stage cancer diagnosis. Extensive simulation studies consistently corroborated the sensor's ability to distinguish between healthy and cancerous cervical tissue. Furthermore, benchmarking against state-of-the-art sensor designs reported in the literature highlighted the proposed sensor's remarkable performance, particularly in terms of absorbance levels and the width of the operating bandwidth. These features make the proposed sensor a suitable tool for high-sensitivity cancer detection.

ACKNOWLEDGMENT

Musa N. Hamza is with the Department of Physics, College of Science, University of Raparin, Sulaymaniyah 46012, Iraq (e-mail: musa.nuraden@uor.edu.krd).

Mohammad Tariqul Islam is with the Department of Electrical, Electronic and Systems Engineering, Faculty of Engineering and Built Environment, Universiti Kebangsaan Malaysia (UKM), Bangi, Selangor 43600, Malaysia (e-mail: tariqul@ukm.edu.my).

Sunil Lavadiya is with the Department of Information and Communication Technology, Marwadi University, Rajkot, Gujarat 360003, India (e-mail: sunil.lavadiya@marwadieducation.edu.in).

Iftikhar ud Din is with the Telecommunication Engineering Department, University of Engineering and Technology, Mardan 23200, Pakistan (e-mail: iftikharuddin114@gmail.com).

Bruno Cavalcante de Souza Sanches is with the Department of Electronic Systems Engineering, Escola Politécnica da Universidade de São Paulo, São Paulo 05508-010, Brazil (e-mail: bruno.csanches@usp.br).

Slawomir Koziel is with the Engineering Optimization and Modeling Center, Reykjavik University, 102 Reykjavik, Iceland, and also with the Faculty of Electronics, Telecommunications and Informatics, Gdansk University of Technology, 80-233 Gdansk, Poland (e-mail: Koziel@ru.is).

Syeda Iffat Naqvi is with the Department of Telecommunication Engineering, University of Engineering and Technology, Taxila 47050, Pakistan (e-mail: iffat.naqvi@uettaxila.edu.pk).

Ali Farmani is with the Department of Electronics Engineering, Lorestan University, Khorramabad 68151-44316, Iran (e-mail: farmani.a@lu.ac.ir).

Md. Shabiul Islam is with the Faculty of Engineering (FOE), Multimedia University (MMU), Cyberjaya, Selangor 63100, Malaysia (e-mail: shabiul.islam@mmu.edu.my).

REFERENCES

[1] D.-K. Lee et al., "Nano metamaterials for ultrasensitive terahertz biosensing," *Sci. Rep.*, vol. 7, no. 1, p. 8146, Aug. 2017.

[2] S.-H. Lee et al., "Label-free brain tissue imaging using large-area terahertz metamaterials," *Biosensors Bioelectron.*, vol. 170, Dec. 2020, Art. no. 112663.

[3] A. Ahmadivand, B. Gerislioglu, R. Ahuja, and Y. K. Mishra, "Terahertz plasmonics: The rise of toroidal metadevices towards immunobiosensings," *Mater. Today*, vol. 32, pp. 108–130, Jan. 2020.

[4] X. Zhang et al., "Terahertz surface plasmonic waves: A review," *Adv. Photon.*, vol. 2, no. 1, Jan. 2020, Art. no. 014001.

[5] R. Wang et al., "Triple-band tunable perfect terahertz metamaterial absorber with liquid crystal," *Opt. Exp.*, vol. 25, no. 26, p. 32280, 2017.

[6] W. Yang and Y.-S. Lin, "Tunable metamaterial filter for optical communication in the terahertz frequency range," *Opt. Exp.*, vol. 28, no. 12, p. 17620, 2020.

[7] M. N. Hamza, M. T. Islam, S. Lavadiya, S. Koziel, I. U. Din, and B. C. de Souza Sanches, "Designing a high-sensitivity dual-band nanobiosensor based on petahertz MTMs to provide a perfect absorber for early-stage nonmelanoma skin cancer diagnostic," *IEEE Sensors J.*, vol. 24, no. 11, pp. 18418–18427, Jun. 2024.

[8] F. Li et al., "The terahertz metamaterials for sensitive biosensors in the detection of ethanol solutions," *Opt. Commun.*, vol. 475, Nov. 2020, Art. no. 126287.

[9] M. N. Hamza, M. T. Islam, and S. Koziel, "Advanced sensor for noninvasive breast cancer and brain cancer diagnosis using antenna array with metamaterial-based AMC," *Eng. Sci. Technol., Int. J.*, vol. 56, Aug. 2024, Art. no. 101779.

[10] M. N. Hamza, S. Koziel, and A. Pietrenko-Dabrowska, "Design and experimental validation of a metamaterial-based sensor for microwave imaging in breast, lung, and brain cancer detection," *Sci. Rep.*, vol. 14, no. 1, p. 16177, Jul. 2024.

[11] D. R. Smith, J. B. Pendry, and M. C. K. Wiltshire, "Metamaterials and negative refractive index," *Science*, vol. 305, no. 5685, pp. 788–792, 2004.

[12] H. Ou, F. Lu, Z. Xu, and Y.-S. Lin, "Terahertz metamaterial with multiple resonances for biosensing application," *Nanomaterials*, vol. 10, no. 6, p. 1038, May 2020.

[13] S. Tan, F. Yan, W. Wang, H. Zhou, and Y. Hou, "Ultrasensitive sensing with three-dimensional terahertz metamaterial absorber," *J. Opt.*, vol. 20, no. 5, May 2018, Art. no. 055101.

[14] C. Tan et al., "Cancer diagnosis using terahertz-graphene-metasurface-based biosensor with dual-resonance response," *Nanomaterials*, vol. 12, no. 21, p. 3889, Nov. 2022.

[15] Z. Vafapour, W. Troy, and A. Rashidi, "Colon cancer detection by designing and analytical evaluation of a water-based THz metamaterial perfect absorber," *IEEE Sensors J.*, vol. 21, no. 17, pp. 19307–19313, Sep. 2021.

[16] S. J. Park et al., "Detection of microorganisms using terahertz metamaterials," *Sci. Rep.*, vol. 4, no. 1, p. 4988, May 2014.

[17] S. J. Park, S. H. Cha, G. A. Shin, and Y. H. Ahn, "Sensing viruses using terahertz nano-gap metamaterials," *Biomed. Opt. Exp.*, vol. 8, no. 8, pp. 3551–3558, 2017.

[18] S. Asgari, N. Granpayeh, and T. Fabritius, "Controllable terahertz cross-shaped three-dimensional graphene intrinsically chiral metastructure and its biosensing application," *Opt. Commun.*, vol. 474, Nov. 2020, Art. no. 126080.

[19] T. Chen, D. Zhang, F. Huang, Z. Li, and F. Hu, "Design of a terahertz metamaterial sensor based on split ring resonator nested square ring resonator," *Mater. Res. Exp.*, vol. 7, no. 9, Sep. 2020, Art. no. 095802.

[20] J. Yang and Y.-S. Lin, "Design of tunable terahertz metamaterial sensor with single- and dual-resonance characteristic," *Nanomaterials*, vol. 11, no. 9, p. 2212, Aug. 2021.

[21] H. Hu, B. Qi, Y. Zhao, X. Zhang, Y. Wang, and X. Huang, "A graphene-based THz metasurface sensor with air-spaced structure," *Frontiers Phys.*, vol. 10, Sep. 2022, Art. no. 990126.

[22] E. Hoseini, A. Mir, and A. Farmani, "Modeling and proposal of a black phosphorus-based nanostructure for detection of avian influenza virus in infrared region," *Opt. Quantum Electron.*, vol. 54, no. 10, p. 609, Oct. 2022.

[23] H. Sung et al., "Global cancer statistics 2020: GLOBOCAN estimates of incidence and mortality worldwide for 36 cancers in 185 countries," *CA, Cancer J. Clinicians*, vol. 71, no. 3, pp. 209–249, Feb. 2021.

[24] R. L. Siegel, K. D. Miller, N. S. Wagle, and A. Jemal, "Cancer statistics, 2023," *CA, Cancer J. Clinicians*, vol. 73, no. 1, pp. 17–48, Jan. 2023.

[25] X.-R. Li and Y.-G. Zhou, "Electrochemical detection of circulating tumor cells: A mini review," *Electrochem. Commun.*, vol. 124, Mar. 2021, Art. no. 106949.

[26] S. Lee et al., "Near-infrared heptamethine cyanine based iron oxide nanoparticles for tumor targeted multimodal imaging and photothermal therapy," *Sci. Rep.*, vol. 7, no. 1, p. 2108, May 2017.

[27] M. Y. Azab, M. F. O. Hameed, A. M. Nasr, and S. S. A. Obayya, "Highly sensitive metamaterial biosensor for cancer early detection," *IEEE Sensors J.*, vol. 21, no. 6, pp. 7748–7755, Mar. 2021.

[28] M. N. Hamza and M. T. Islam, "Designing an extremely tiny dual-band biosensor based on MTMs in the terahertz region as a perfect absorber for non-melanoma skin cancer diagnostics," *IEEE Access*, vol. 11, pp. 136770–136781, 2023.

[29] S. K. Patel, J. Surve, and J. Parmar, "Detection of cancer with graphene metasurface-based highly efficient sensors," *Diamond Rel. Mater.*, vol. 129, Nov. 2022, Art. no. 109367.

[30] B. Amini and Z. Atlasbaf, "Design and analysis of high-sensitivity tunable graphene sensors for cancer detection," *Opt. Quantum Electron.*, vol. 55, no. 5, p. 446, May 2023.

[31] M. N. Hamza and M. T. Islam, "Design of MTM-based multiband micro-biosensor in terahertz region as perfect absorber for early-stage leukemia diagnosis with sensitivity 18 626 373 THz/RIU," *IEEE Sensors J.*, vol. 24, no. 10, pp. 16055–16069, May 2024.

[32] P. Upender and A. Kumar, "THz dielectric metamaterial sensor with high Q for biosensing applications," *IEEE Sensors J.*, vol. 23, no. 6, pp. 5737–5744, Mar. 2023.

[33] Z. Geng, X. Zhang, Z. Fan, X. Lv, and H. Chen, "A route to terahertz metamaterial biosensor integrated with microfluidics for liver cancer biomarker testing in early stage," *Sci. Rep.*, vol. 7, p. 16378, Nov. 2017.

[34] M. N. Hamza et al., "Designing a high-sensitivity microscale triple-band biosensor based on terahertz MTMs to provide a perfect absorber for non-melanoma skin cancer diagnostic," *IEEE Photon. J.*, vol. 16, no. 2, pp. 1–13, Apr. 2024.

[35] S. Banerjee, U. Nath, P. Dutta, A. V. Jha, B. Appasani, and N. Bizon, "A theoretical terahertz metamaterial absorber structure with a high quality factor using two circular ring resonators for biomedical sensing," *Inventions*, vol. 6, no. 4, p. 78, Nov. 2021.

[36] H. E. Nejad, A. Mir, and A. Farmani, "Supersensitive and tunable nano-biosensor for cancer detection," *IEEE Sensors J.*, vol. 19, no. 13, pp. 4874–4881, Jul. 2019.

[37] M. N. Hamza et al., "A very compact metamaterial-based triple-band sensor in terahertz spectrum as a perfect absorber for human blood cancer diagnostics," *Plasmonics*, vol. 19, no. 5, pp. 1–14, May 2024.

[38] D. Li et al., "Identification of early-stage cervical cancer tissue using metamaterial terahertz biosensor with two resonant absorption frequencies," *IEEE J. Sel. Topics Quantum Electron.*, vol. 27, no. 4, pp. 1–7, Jul. 2021.

[39] Z. Chen et al., "Graphene multi-frequency broadband and ultra-broadband terahertz absorber based on surface plasmon resonance," *Electronics*, vol. 12, no. 12, p. 2655, Jun. 2023.

[40] Z. EL-Wasif, T. Ismail, and O. Hamdy, "Design and optimization of highly sensitive multi-band terahertz metamaterial biosensor for coronaviruses detection," *Opt. Quantum Electron.*, vol. 55, no. 7, p. 604, Jul. 2023.

[41] M.-R. Nickpay, M. Danaie, and A. Shahzadi, "Highly sensitive THz refractive index sensor based on folded split-ring metamaterial graphene resonators," *Plasmonics*, vol. 17, no. 1, pp. 237–248, Feb. 2022.

[42] Y. Wang et al., "Terahertz tunable three band narrowband perfect absorber based on dirac semimetal," *Phys. E, Low-Dimensional Syst. Nanostruct.*, vol. 131, Jul. 2021, Art. no. 114750.

[43] B.-X. Wang, Y. He, P. Lou, and W. Xing, "Design of a dual-band terahertz metamaterial absorber using two identical square patches for sensing application," *Nanosc. Adv.*, vol. 2, no. 2, pp. 763–769, 2020.

[44] S. Zhuang et al., "Graphene-based absorption–transmission multi-functional tunable THz metamaterials," *Micromachines*, vol. 13, no. 8, p. 1239, Aug. 2022.

[45] S. Asgari and T. Fabritius, "Numerical simulation and equivalent circuit model of multi-band terahertz absorber composed of double-sided graphene comb resonator array," *IEEE Access*, vol. 11, pp. 36052–36063, 2023.

[46] L. Liu, W. Liu, and Z. Song, "Ultra-broadband terahertz absorber based on a multilayer graphene metamaterial," *J. Appl. Phys.*, vol. 128, no. 9, pp. 093104-1–093104-6, Sep. 2020.

[47] A. S. Saadeldin, M. F. O. Hameed, E. M. A. Elkaramany, and S. S. A. Obayya, "Highly sensitive terahertz metamaterial sensor," *IEEE Sensors J.*, vol. 19, no. 18, pp. 7993–7999, Sep. 2019.

[48] L. Angrisani, G. Cavallo, A. Liccardo, G. P. Papari, and A. Andreone, "THz measurement systems," in *New Trends and Developments in Metrology*. London, U.K.: InTech, 2016, pp. 21–48.

[49] A. Steiger, M. Kehrt, C. Monte, and R. Müller, "Traceable terahertz power measurement from 1 THz to 5 THz," *Opt. Exp.*, vol. 21, no. 12, p. 14466, 2013.
[50] C. Chong, H. Liu, S. Wang, S. Chen, and H. Xie, "Sensitivity analysis of biosensors based on a dielectric-modulated L-shaped gate field-effect transistor," *Micromachines*, vol. 12, no. 1, p. 19, Dec. 2020.
[51] G. Wadhwa and B. Raj, "Design, simulation and performance analysis of JLTFET biosensor for high sensitivity," *IEEE Trans. Nanotechnol.*, vol. 18, pp. 567–574, 2019.
[52] M. K. Anvarifard, Z. Ramezani, I. S. Amiri, K. Tamersit, and A. M. Nejad, "Profound analysis on sensing performance of nanogap SiGe source DM-TFET biosensor," *J. Mater. Sci., Mater. Electron.*, vol. 31, no. 24, pp. 22699–22712, Nov. 2020.
[53] S. Kumar, Y. Singh, B. Singh, and P. K. Tiwari, "Simulation study of dielectric modulated dual channel trench gate TFET-based biosensor," *IEEE Sensors J.*, vol. 20, no. 21, pp. 12565–12573, Nov. 2020.
[54] S. Hannan, M. T. Islam, A. F. Almutairi, and M. R. I. Faruque, "Wide bandwidth angle- and polarization-insensitive symmetric metamaterial absorber for X and Ku band applications," *Sci. Rep.*, vol. 10, no. 1, p. 10338, Jun. 2020.
[55] K. V. Babu, P. Das, S. Das, A. H. M. Almawgani, T. Islam, and A. R. H. Alhawari, "Design of graphene-based broadband metamaterial absorber with circuit analysis approach for terahertz region applications," *Opt. Quantum Electron.*, vol. 55, no. 13, p. 1188, Dec. 2023.
[56] N. Misran, S. H. Yusop, M. T. Islam, and M. Y. Ismail, "Analysis of parameterization substrate thickness and permittivity for concentric split ring square reflectarray element," *Jurnal Kejuruteraan, J. Eng.*, vol. 23, pp. 11–16, Nov. 2012.
[57] F. Caspers, "RF engineering basic concepts: S-parameters," 2012, *arXiv:1201.2346*.
[58] K. Ahmed, B. K. Paul, F. Ahmed, M. A. Jabin, and M. S. Uddin, "Numerical demonstration of triangular shaped photonic crystal fibre-based biosensor in the terahertz range," *IET Optoelectronics*, vol. 15, no. 1, pp. 1–7, Feb. 2021.
[59] M. A. Jabin et al., "Surface plasmon resonance based titanium coated biosensor for cancer cell detection," *IEEE Photon. J.*, vol. 11, no. 4, pp. 1–10, Aug. 2019.
[60] P. Kumar, V. Kumar, and J. S. Roy, "Dodecagonal photonic crystal fibers with negative dispersion and low confinement loss," *Optik*, vol. 144, pp. 363–369, Sep. 2017.
[61] T. Parvin, K. Ahmed, A. M. Alatwi, and A. N. Z. Rashed, "Differential optical absorption spectroscopy-based refractive index sensor for cancer cell detection," *Opt. Rev.*, vol. 28, no. 1, pp. 134–143, Feb. 2021.
[62] P. Sharma, P. Sharan, and P. Deshmukh, "A photonic crystal sensor for analysis and detection of cancer cells," in *Proc. Int. Conf. Pervasive Comput. (ICPC)*, Jan. 2015, pp. 1–5.
[63] A. Rehman, S. Firdous, M. Nawaz, and M. Ahmad, "Optical parameters measurement for diagnostic and photodynamic therapy of human cervical adenocarcinoma (HeLa) cell line," *Laser Phys.*, vol. 22, no. 1, pp. 322–326, Jan. 2012.
[64] R. Bhati and A. K. Malik, "Ultra-efficient terahertz metamaterial sensor," *Results Opt.*, vol. 8, Aug. 2022, Art. no. 100236.
[65] Y. Shen et al., "Low-concentration biological sample detection using an asymmetric split resonator terahertz metamaterial," *Photonics*, vol. 10, no. 2, p. 111, Jan. 2023.
[66] Z. Mezache, Z. Hafdi, and J. Tao, "Design of a novel graphene buzzle metamaterial refractometer for sensing of cancerous cells in the terahertz regime," *Optik*, vol. 287, Sep. 2023, Art. no. 171170.

Musa N. Hamza received the B.Sc. degree from the Department of Physics, Faculty of Science and Health, Koya University, Koya, Iraq, in 2015, and the M.Sc. degree from the Department of Medical Physics, College of Medical and Applied Sciences, Charmo University, Sulaymaniyah, Iraq, in 2023.

His research interests include medical physics, the diagnosis of different types of cancer at an early stage, antenna arrays, metamaterials, sensors, and biosensors.

Mohammad Tariqul Islam (Senior Member, IEEE) is currently a Professor with the Department of Electrical, Electronic and Systems Engineering, Universiti Kebangsaan Malaysia (UKM), Bangi, Malaysia, and a Visiting Professor with the Kyushu Institute of Technology, Fukuoka, Japan. He is the author and co-author of about 600 research journal articles, nearly 250 conference papers, and a few book chapters on various topics related to antennas, metamaterials, and microwave imaging with 25 inventory patents filed. Thus far, his publications have been cited 15 700 times and his H-index is 56 (Source: Scopus). His Google scholar citation is 25 000 and H-index is 66. He was a recipient of more than 40 research grants from the Malaysian Ministry of Science, Technology and Innovation, Ministry of Education, UKM research grant, and international research grants from Japan, Saudi Arabia, and Kuwait. His research interests include communication antenna design, metamaterial, satellite antennas, and microwave imaging.

Dr. Islam has been serving as an Executive Committee Member for IEEE AP/MTT/EMC Malaysia Chapter from 2019 to 2020; the Chartered Professional Engineer (CEng); a Fellow of IET, U.K.; and a Senior Member of IEICE, Japan. He received several international gold medal awards, the Best Invention in Telecommunication Award for his research and innovation, and Best Researcher Awards at UKM. He was a recipient of the 2018, 2019, and 2020 IEEE AP/MTT/EMC Malaysia Chapter, Excellent Award. He also won the Best Innovation Award and the Best Researcher Award by UKM, in different years. He was a recipient of a Publication Award from the Malaysian Space Agency for several years. He has supervised about 50 Ph.D. theses and 30 M.Sc. theses and has mentored more than ten postdocs and visiting scholars. He has developed the Antenna Measurement Laboratory, which includes antenna design and measurement facility until 40 GHz. He was an Associate Editor of IET *Electronics Letter*. He also serves as a Guest Editor for *Sensors* journal and *Nanomaterials* and an Associate Editor for IEEE ACCESS.

Sunil Lavadiya (Member, IEEE) received the B.Tech. degree in electronics and communication from Saurashtra University, Rajkot, India, in 2008, the M.Tech. degree in communication engineering from Nirma University, Ahmedabad, India, in 2010, and the Ph.D. degree in electronics and communication engineering from Marwadi University, Rajkot, India, in 2022.

He working as an Associate Professor with the Department of Information and Communication Technology, Marwadi University. He has adapted to all aspects of Electronics and Communication Engineering, including training, education, and research. He works in the MIMO, sensors, reconfigurable, superstrate, solar absorber, and liquid antennas. He has published 50 SCI research articles, 12 Scopus index articles, eight book chapters, and five papers in an international conference and filed four design patents and one copyright.

Dr. Lavadiya is a member of IETE.

Iftikhar ud Din received the B.Sc. and M.Sc. degrees in telecommunication engineering from the University of Engineering and Technology, Peshawar, Pakistan, in 2017 and 2021, respectively.

His current research interests include UWB antennas, FSS-based UWB antennas and sub-6-GHz 5G antennas, 5G millimeter-wave antennas and MIMO antennas, frequency selective surfaces, EBGs, and metamaterial-based antenna.

Dr. ud Din is a member of the Antennas and Microwave Engineering Research Group (AMERG), UET, Mardan, Pakistan.

Bruno Cavalcante de Souza Sanches (Member, IEEE) received the B.S. degree in information engineering and the M.Sc. degree in energy from the Federal University of ABC, Santo André, Brazil, in 2011 and 2013, respectively, and the Ph.D. degree in microelectronics with the Integrated Systems Laboratory (LSI), University of São Paulo, São Paulo, Brazil, in 2021.

He is working on the design of a novel mixed-signal integrated circuit used in the ALICE experiment in the CERN LHC. He has more than 15 years of experience in electronics and microelectronics design. He has been involved in hardware development, smart grids, algorithms, artificial intelligence, digital communication systems, EDA tools, electronics for high-energy physics experiments, and several systems targeting early cancer detection including bioimpedance spectroscopy and microwave imaging.

Slawomir Koziel (Fellow, IEEE) received the M.Sc. and Ph.D. degrees in electronic engineering from Gdansk University of Technology, Gdansk, Poland, in 1995 and 2000, respectively, and the M.Sc. degree in theoretical physics and the M.Sc. and Ph.D. degrees in mathematics from the University of Gdansk, Gdansk, in 2000, 2002, and 2003, respectively.

He is currently a Professor with the Department of Engineering, Reykjavik University, Reykjavik, Iceland. His research interests include CAD and modeling of microwave and antenna structures, simulation-driven design, surrogate-based optimization, space mapping, circuit theory, analog signal processing, evolutionary computation, and numerical analysis.

Syeda Iffat Naqvi (Senior Member, IEEE) received the Ph.D. degree in telecommunication engineering from the University of Engineering and Technology, Taxila, Pakistan, in 2021.

She is currently serving as an Assistant Professor with the University of Engineering and Technology. She is working toward the design and implementation of MIMO antenna systems for millimeter-wave 5G and beyond wireless communication applications, metamaterials, terahertz and sub-terahertz antennas, beamsteerable antenna arrays, and ridge gap waveguide antennas. She has authored and co-authored numerous technical articles in ISI-indexed journals and has delivered several conference talks.

Dr. Naqvi is a frequent reviewer of various prestigious journals. Furthermore, she has served as a technical committee member for several international conferences and as a guest editor for various special journal issues.

Ali Farmani (Member, IEEE) received the B.Sc. degree in electrical engineering from Shiraz University of Technology, Shiraz, Iran, in 2008, the M.Sc. degree in electrical engineering from the University of Tabriz, Tabriz, Iran, in 2010, and the Ph.D. degree in electrical engineering from Shiraz University, Shiraz, in 2017.

Since 2018, he has been stayed at Lorestan University, Khorramabad, Iran, as an Assistant Professor. He has mentored several B.Sc., ten M.Sc. theses, and four Ph.D. dissertations. He is the author of more than 106 ISI papers and three book chapters. His research interests include VLSI, nanoelectronics, plasmonics, and the investigation of new materials for integrated photonics.

Dr. Farmani was a recipient of the fellowship for Ph.D. study at Shiraz University as an Exceptional Talent. He received the Shiraz Distinguished Ph.D. Dissertation Award for his work on plasmonic nanostructures. He has been a recipient of the Excellent Reviewer Award from Elsevier and IEEE Journals, since 2017.

Md. Shabiul Islam (Senior Member, IEEE) received the B.Sc. (Hons.) and M.Sc. degrees from the Department of Applied Physics and Electronics, Rajshahi University, Rajshahi, Bangladesh, in 1985 and 1986, respectively, the M.Sc. degree (by research) in microcontroller-based system design from the Department of Electrical, Electronics and System Engineering, Universiti Kebangsaan Malaysia (UKM), Bangi, Malaysia, in 1997, and the Ph.D. degree in VLSI design from the Faculty of Engineering (FOE), Multimedia University (MMU), Cyberjaya, Malaysia, in 2008.

From 1991 to 1993, he was a Scientific Officer with the Institute of Electronics and Material Science (IEMS), Bangladesh Atomic Energy Commission (BAEC), Saver, Dhaka, Bangladesh. From July 1999 to 2009, he was a Lecturer at the Faculty of Engineering, MMU. From July 2009 to March 2012, he was a Senior Lecturer with the Institute of Microengineering and Nanoelectronics (IMEN), UKM. From June 2010 to December 2012, he was an Associate Fellow with the Department of Electrical, Electronics and System Engineering, Faculty of Engineering and Built Environment, UKM. From March 2012 to December 2016, he worked as an Associate Professor with IMEN, where he was an Associate Fellow, from April 2017 to March 2020. He is currently a Professor with the Faculty of Engineering, MMU. He is also the Head of the Micro/Nano Electronics System (MiNES) Laboratory, IMEN. His expertise covers a wide range of engineering disciplines, including micro/nano system design, VLSI design, microcontroller-based system design, micro-powering harvesting, and digital communication systems. He received internal and external research funds for doing research work at IMEN from 2010 to 2016. His research support also partly contributed to the award of the Higher Education Center of Excellence (HiCOE) from the Malaysian Government to IMEN recently. He has published 78 ISI and Scopus, five research books, one chapter in a book, and 90 conference proceedings. He filed one patent.

Dr. Islam is a member of the IEEE Circuits and Systems Society, a member of the Bangladesh Electronics Society, and an Associate Member of Bangladesh Computer Society (AM476).